# CALCULATION OF COMPRESSIBLE AND INCOMPRESSIBLE VISCOUS FLOWS BY A VISCOUS INVISCID SPLITTING FINITE ELEMENT METHOD

**Jichao Su**
**Aerodynamics Laboratory, Institute for Aerospace Research,**
**National Research Council Canada, Ottawa, Ontario, Canada K1A 0R6**

**Keywords**: *finite element method, zonal method, viscous flow, potential flow*

## Abstract

*A viscous-inviscid splitting finite element method is developed to solve two-dimensional compressible and incompressible external flows. The outer inviscid solution is dealt with by solving the potential flow using an artificial compressibility finite element method while the inner viscous solution is obtained by solving the Navier-Stokes equations by a streamline upwind Petrov-Galerkin finite element method. The motivation of developing this approach is to take full advantage of the physical nature of the flow around aircraft where in most cases, the viscous effects are substantial only in the vicinity of the aircraft surface and its wake. Some preliminary results for the two dimensional compressible and incompressible flows around an NACA0012 airfoil are presented to show the efficiency and accuracy of the method.*

## 1 Introduction

The solution for the viscous flow around aircraft has been computed by a variety of numerical methods including viscous-inviscid splitting methods [1-3]. The viscous-inviscid splitting methods, which were more or less boundary-layer-like in the early stages of development, are becoming increasingly Navier-Stokes-like so that separations and shock wave boundary layer interactions can be handled. These methods actually create a new way to develop Navier-Stokes solvers that benefit from the numerical conditioning of the boundary layer techniques. By taking full advantage of physical nature of the flow, they also provide the best way to get approximate solvers that substantially reduce the computer cost by simplifying the governing equations [4,5].

Viscous-inviscid splitting methods do not necessarily involve approximations. They can be classified into three types:

*Zonal methods*: In these methods, the computational domain is divided into an inviscid zone where an inviscid solver is used and a viscous zone near the body surface and its wake where a Navier-Stokes solver is employed. The computational efficiency is thus improved by reducing the extent of the viscous computational domain [6,7]. However, the resulting zonal Navier-Stokes solver has to be coupled with the outer inviscid solver along a patching boundary, located in the inviscid part of the flow.

*Thin-Layer methods*: These methods can be regarded as an extrapolation of the approximations and techniques of the boundary layer by viscous-inviscid coupling. Solvers with low cost are generated based on approximate momentum equations. Because such solvers are Navier-Stokes-like if the coupling is strong and numerically consistent, they may provide the capability to compute complex flows with multiple viscous interactions.

*Composite methods*: The idea of these methods is an extension of the second type. These methods maintain the splitting into an inviscid-like predictor problem plus a viscous-corrector problem with overlaying

computational domains. They intend to benefit from fast marching solutions for the viscous part and to couple the predictor and corrector problems by iterative numerical methods [5,8].

In the present paper, a zonal finite element method is developed to deal with two dimensional compressible and incompressible external flows. The outer inviscid solution is computed by solving the potential flow using an artificial compressibility finite element method. The inner viscous solution is obtained by solving the Navier-Stokes equations by a streamline upwind Petrov-Galerkin finite element method.

## 2 Numerical Method

### 2.1 Navier-Stokes inner viscous solution method

We consider two-dimensional compressible and incompressible viscous flows around an airfoil. The governing equations take the following form:

*Continuity equation*

$$\frac{\partial \rho}{\partial t}+\frac{\partial(\rho u_i)}{\partial x_i}=0 \tag{1}$$

*Momentum equations*

$$\frac{\partial(\rho u_j)}{\partial t}+\frac{\partial(\rho u_i u_j)}{\partial x_i}=-\frac{\partial p}{\partial x_j}+\frac{\partial t_{ij}}{\partial x_j} \quad (j=1,2) \tag{2}$$

*Energy equation*

$$\frac{\partial}{\partial t}\left[\rho\left(e+\frac{1}{2}u_i u_i\right)\right]+\frac{\partial}{\partial x_j}\left[\rho u_j\left(h+\frac{1}{2}u_i u_i\right)\right] =\frac{\partial(u_i t_{ij})}{\partial x_j}-\frac{\partial q_j}{\partial x_j} \tag{3}$$

where $e=C_\upsilon T$ is specific internal energy and $C_\upsilon$ is the specific heat coefficient; $h=e+p/\rho$ is specific enthalpy; the repeated indices indicate summation. The heat flux vector $q_j$ is governed by Fourier's law

$$q_j=-\kappa\frac{\partial T}{\partial x_j} \quad (j=1,2) \tag{4}$$

where $\kappa$ is thermal conductivity. The perfect gas law

$$p=\rho RT \tag{5}$$

and the constitute relation between stress and strain rate

$$t_{ij}=2\mu S_{ij}-\frac{2}{3}\mu\frac{\partial u_k}{\partial x_k}\delta_{ij};\qquad S_{ij}=\frac{1}{2}\left(\frac{\partial u_i}{\partial x_j}+\frac{\partial u_j}{\partial x_i}\right) \tag{6}$$

close the above system. Here $R$ is the perfect gas constant and $\delta_{ij}$ is the Kronecker delta. The thermal conductivity is determined by $\kappa=\frac{\gamma}{\gamma-1}R\mu/Pr$ where $Pr$ is the Prandtl number and $\gamma$ is the ratio of specific heats.

We divide $\rho u_j$ in the time interval from $t_n$ to $t_n+dt$ as

$$\rho u_j(x_1,x_2,t)=(\rho u_j)_n(x_1,x_2)+\Delta(\rho u_j)^*(x_1,x_2,t)+\Delta(\rho u_j)^{**}(x_1,x_2,t) \quad (j=1,2) \tag{7}$$

and the pressure $p$ is expressed as

$$p(x_1,x_2,t)=p_n(x_1,x_2)+\Delta p(x_1,x_2,t) \tag{8}$$

where $\Delta(\rho u_j)^*, \Delta(\rho u_j)^{**}$ $(j=1,2)$ and $\Delta p$ are incremental values. Substituting equations (7) and (8) in the momentum equation (2), we split the equation into two equations as

$$\frac{\partial(\Delta(\rho u_j)^*)}{\partial t}+\frac{\partial(\rho u_i u_j)}{\partial x_i} =-\frac{\partial p_n}{\partial x_j}+\frac{\partial t_{ij}}{\partial x_j} \quad (j=1,2) \tag{9}$$

$$\frac{\partial(\Delta(\rho u_j)^{**})}{\partial t}+\frac{\partial(\Delta p)}{\partial x_j}=0 \tag{10}$$

From equation (10), we note that $\Delta(\rho u_j)^{**}$ is associated with the increment of pressure $p$. This equation may be regarded to the momentum equation as a correction equation that ensures the satisfaction of mass continuity.

Equation (9) with the initial and boundary conditions may be solved by an explicit or semi-implicit Taylor-expansion algorithm [9,10]. However since the time step for the explicit algorithm or semi-implicit is quite limited, especially when a fine mesh is needed to obtain accurate results, a fully implicit algorithm is developed for the solution of equation (9). Discretizing equation (9) in time, we obtain

$$\Delta(\rho u_j)^*_{n+1} - \theta\Delta t\,\nu\nabla^2(\Delta(\rho u_j)^*_{n+1}) + \theta\Delta t\frac{\partial[(u_i)_n\Delta(\rho u_j)^*_{n+1}]}{\partial x_i} + \theta\Delta t\frac{\partial[(u_j)_n\Delta(\rho u_i)^*_{n+1}]}{\partial x_i} = -\Delta t\left[\frac{\partial(\rho u_i u_j)_n}{\partial x_i} + \frac{\partial p_n}{\partial x_j} - \frac{\partial(t_{ij})_n}{\partial x_j}\right] (j=1,2) \quad (11)$$

Equation (11) is then solved by a streamline upwind Petrov-Galerkin finite element method [15].

The prescribed velocity boundary condition is implemented on the first part of the solution. That is

$$\Delta(\rho u_j)^* = (\overline{\rho u})_j(x_1,x_2,t) - (\overline{\rho u})_j(x_1,x_2,t_n) \quad (j=1,2) \text{ on } \partial\Omega \quad (12)$$

where $\partial\Omega$ is the boundary of the fluid domain of investigation $\Omega$ and $\overline{\rho u_j}$ denotes the prescribed value on the boundary. For the second part of the solution we impose homogeneous boundary conditions, namely,

$$\Delta(\rho u_j)^{**} = 0 \ (j=1,2) \quad \text{on } \partial\Omega \quad (13)$$

so that the combination of the two parts of the solution satisfies the given physical boundary conditions.

Equation (10) is not sufficient to determine $\Delta(\rho u_j)^{**}$ $(j=1,2)$. The continuity equation, i.e. equation (1), is required for the solution of $\Delta(\rho u_j)^{**}$. Thus, for the solution of $\Delta(\rho u_j)^{**}$ and $\Delta p$, we need

$$\frac{\partial\rho}{\partial t} + \frac{\partial(\rho u_i)}{\partial x_i} = 0 \quad (14)$$

$$\frac{\partial(\Delta(\rho u_j)^{**})}{\partial t} + \frac{\partial(\Delta p)}{\partial x_j} = 0 \quad (15)$$

After discretizing the above equations in time and a little derivation, we obtain

$$\frac{1}{RT_n}(\Delta p)_{n+1} - (\theta\Delta t)^2\nabla^2(\Delta p)_{n+1} = -\Delta t\left[\frac{\partial(\rho u_i)_n}{\partial x_i} + \theta\frac{\partial(\Delta(\rho u_i)^*_{n+1})}{\partial x_i}\right] \quad (16)$$

$$\Delta(\rho u_j)^{**}_{n+1} = -\theta\Delta t\frac{\partial(\Delta p)_{n+1}}{\partial x_j} \quad (j=1,2) \quad (17)$$

These two equations with boundary conditions

$$\Delta(\rho u_j)^{**}_{n+1} = 0 \quad (j=1,2) \text{ on } \partial\Omega \quad (18)$$

$$\frac{\partial(\Delta p)_{n+1}}{\partial n} = 0 \quad (19)$$

determine the solution of $\Delta(\rho u_j)^{**}$ and $\Delta p$. The discretization of equation (3) is similar to equation (9).

When turbulent flows are considered, a turbulence model is introduced, the viscosity $\mu$ in equation (2) and (3) is replaced by $\mu+\mu_T$ where $\mu_T$ is the eddy viscosity as defined below, and $\kappa$ is replaced by $\kappa+\kappa_T$ where $\kappa_T = \frac{\gamma}{\gamma-1}R\mu_T/Pr_T$ and $Pr_T$ is the turbulent Prandtl number.

For turbulent flows, the Spalart-Allmaras one equation model is employed for modeling the eddy viscosity [16]. Its defining equations are as follows:

*Kinematic eddy viscosity*

$$\nu_T = \bar{\nu} f_{\upsilon 1}\ ; \quad \mu_T = \rho\nu_T \quad (20)$$

*Eddy viscosity equation*

$$\frac{\partial\bar{\nu}}{\partial t} + \frac{\partial(u_i\bar{\nu})}{\partial x_i} = c_{b1}\bar{S}\bar{\nu} - c_{w1}f_w\left(\frac{\bar{\nu}}{d}\right)^2 + \frac{1}{\sigma}\frac{\partial}{\partial x_i}\left[(\nu+\bar{\nu})\frac{\partial\bar{\nu}}{\partial x_i}\right] + \frac{c_{b2}}{\sigma}\frac{\partial\bar{\nu}}{\partial x_i}\frac{\partial\bar{\nu}}{\partial x_i} \quad (21)$$

*Closure coefficients*

$$c_{b1}=0.1355,\ c_{b2}=0.622,\ c_{\upsilon 1}=7.1,\ \sigma=2/3,\ c_{w1}=\frac{c_{b1}}{\kappa^2}+\frac{(1+c_{b2})}{\sigma},\ c_{w2}=0.3,\ c_{w3}=2,\ \kappa=0.41 \quad (22)$$

*Auxiliary relations*

$$f_{\upsilon 1}=\frac{\chi^3}{\chi^3+c_{\upsilon 1}^3},\quad f_{\upsilon 2}=1-\frac{\chi}{1+\chi f_{\upsilon 1}},\quad f_w=g\left[\frac{1+c_{w3}^6}{g^6+c_{w3}^6}\right]^{1/6},\ \chi=\frac{\bar{\nu}}{\nu}, \quad (23a)$$

$$g = r + c_{w2}(r^6 - r),\ r = \frac{\bar{\nu}}{\bar{S}\kappa^2 d^2},$$

$$\bar{S} = S + \frac{\bar{\nu}}{\kappa^2 d^2} f_{\upsilon 2},\ S = \sqrt{2\Omega_{ij}\Omega_{ij}}, \qquad (23b)$$

$$\Omega_{ij} = \frac{1}{2}\left(\frac{\partial u_i}{\partial x_j} - \frac{\partial u_j}{\partial x_i}\right)$$

where $d$ is the distance from the closest surface; the kinematic viscosity $\nu = \mu/\rho$. The time discretization of equation (21) is similar to that of equation (9).

## 2.2 Potential outer inviscid solution method

The full potential equation is the continuity equation (1) with the velocity defined as

$$u_j = (u_j)_\infty + \frac{\partial \phi}{\partial x_j} \qquad (24)$$

and density and pressure determined by

$$\rho = \rho_\infty \left[1 + \frac{\gamma - 1}{2} M_\infty^2 \left(1 - \frac{V^2 + 2\phi_t}{V_\infty^2}\right)\right]^{1/(\gamma-1)} \qquad (25)$$

$$p = p_\infty \left[1 + \frac{\gamma - 1}{2} M_\infty^2 \left(1 - \frac{V^2 + 2\phi_t}{V_\infty^2}\right)\right]^{\gamma/(\gamma-1)} \qquad (26)$$

where $(u_j)_\infty$ and $\phi(x_1, x_2, t)$ are the freestream velocity and the perturbation velocity potential, respectively. For the incompressible flow, the density $\rho$ is constant. Thus the perturbation potential satisfies the Laplace equation. The boundary conditions for equations (1) and (24) are:

1. The perturbation velocity potential in the farfield (except at the outflow) is set zero;
2. The flux through the outflow is set equal to the freestream flux. This condition allows a jump in the velocity potential at the outflow on the wake;
3. At any location on a prescribed wake sheet there are two values for $\phi$, so two conditions must be imposed. First, the mass flux through the wake is continuous and second, the pressures on the upper and lower wake must be equal. This condition is required only when the whole flow field is chosen as an inviscid potential zone.

An artificial compressibility Galerkin finite element method was developed to solve the above potential flow problem [17].

## 2.3 Matching of the inner viscous and outer inviscid solutions

The interfaces that separate the inviscid and viscous zones are located in the physically inviscid domain and actually have two adjacent surfaces. The velocity, pressure and temperature are matched on these surfaces so that the potential governing equation is satisfied on the one surface while the viscous Navier-Stokes equations including energy equation are satisfied on the other surface.

## 3 Numerical Implementation

A finite element method is employed to further discretize the governing equations in space after the time discretization. Here we take equation (11) for example. A weak formulation is obtained by taking a scalar product with an appropriate weighting function and integrating over the domain $\Omega$. Then for discretization of the weak formulation we may use different or the same interpolation approximations for both velocity and pressure. In the present study, we use bilinear approximations for all variables. The interpolations are expressed as

$$\rho u_j(x_1, x_2) = \sum_{i=1}^{\bar{N}} U_i(x_1, x_2)(\rho u_j)_i \ (j = 1,2) \qquad (27)$$

$$p(x_1, x_2) = \sum_{i=1}^{\bar{M}} \Pi_i(x_1, x_2)\, p_i \qquad (28)$$

where $\bar{N}$ is the total number of nodes for the velocity components; $\bar{M}$ is the total number of nodes for the pressure; $(\rho u_j)_i$ and $p_i$ are the nodal variables; $U_i(x_1, x_2)$ and $\Pi_i(x_1, x_2)$ are node functions. By using equations (27) and (28) and setting the weighting function the same as the corresponding node function (with upwind modification for the Petrov-Galerkin method), we can derive a finite element algebraic system of equations which is solved for the solution. A similar procedure is used with equations (18) and (19) for $\Delta(\rho u_j)^{**}$ and

$\Delta p$, equations (20) and (21) for eddy viscosity, equations (1) and (24) for the velocity potential, and equation (3) for $T$.

## 4 Numerical Results

Some preliminary results are presented for two-dimensional compressible and incompressible flows around the NACA0012 airfoil. A C-type grid near the airfoil is shown in figure 1. When the whole grid is chosen as an inviscid zone, either a potential or Euler solution ($\mu = 0$) is obtained. The full Navier-Stokes solution is calculated when the whole grid is chose as a viscous zone.

Figure 2 (where $X$ is defined as $x_1/c$ and c is the airfoil chord length) shows the pressure coefficient on the surface of the airfoil with $0^o$ angle of attack and Mach numer $M_\infty = 0.0$. It is noted that the present potential solution and Euler solution are in close agreement with the data (potential result) from [11]. Although the grid is not fine, the difference between the potential and Euler solutions is almost indiscernible for this case. The full Navier-Stokes and zonal solutions are also given in the figure for the viscous flow with a Reynolds number (Re) of 6000. The agreement is very good. The difference between inviscid and viscous solutions is quite obivious and expected since the Reynolds number is quite low. The results for $2^o$ of angle of attack, $M_\infty = 0.0$ and Re=6000 are presented in figure 3 together with the corresponding potential and Euler solutions. There is near the airfoil leading edge a noticeable difference between the potential and Euler solutions. The author believes that a finer grid near the leading edge will resolve the difference. Again the full Navier-Stokes and zonal solutions are in excellent agreement for the viscous flow.

The numerical results for compressible flows around the NACA0012 airfoil are shown in figures 4 and 5. For the case of zero angle of attack, $M_\infty$=0.85 and Re=2000, while the potential and Euler solutions are in fairly reasonable agreement as shown in figure 4, the result by the zonal method matches very well the full Navier-Stokes result which also is in fairly good agreement with the full Navier-Stokes finite element results by Elkadri *et al* [12] and Dutto *et al* [13]. The same conclusion can be drawn from the numerical results shown in figure 5 for the case of $1.25^o$ of angle of attack, $M_\infty$=0.80 and Re=2000. It is also noticed from figure 5 that the present Euler solution matches fairly well the corresponding Euler results in reference [12,14].

It is observed from figure 6 that the time histories of the velocity increment defined as

$$\sqrt{\sum_{i=1}^{\bar{N}} \sum_{j=1}^{2} [(\Delta u_j)_i]^2}$$

by both the full Navier-Stokes and zonal methods are in fairly good agreement for incompressible viscous flows. This suggests that the time accuracy of the zonal method is similar to the full Navier-Stokes method for incompressible flows, at least for the present cases. Some numerical oscillations are observed from figure 7 ($\bar{t} = V_\infty / c > 8$ where $V_\infty$ is upstream flow speed) for the two compressible cases. These oscillations may be attributed by the numerical oscillations of potential solutions.

From the above discussion, we can conclude that the overall agreement between the full Navier-Stokes and zonal method is very good. However about 50% of computational time is saved by using the zonal method for both the present two dimensional compressible and incompressible cases.

## 5 Conclusion

A zonal finite element method has been developed in the present paper to simulate two dimensional compressible and incompressible external flows. The outer inviscid flow is dealt with by using an artificial compressibility Galerkin finite element method for potential flow while the inner viscous flow is simulated by using a streamline upwind Petrov-Galerkin finite element method for solving the Navier-Stokes equations. Some preliminary results have been presented for the two-dimensional flows around an NACA0012 airfoil. The results by the present zonal method are in close agreement

with the full Navier-Stokes solutions by the present paper and others. However substantial computational cost is saved by using the zonal method. It is expected more efficiency may be achieved for three dimensional external compressible and incompressible flows.

## References


[1] Metha U and Lomax H. Reynolds-averaged Navier-Stokes computations of transonic flows. The state of the art. *Proceedings of Symposium on Transonic Perspective*, ed. Nixon D, Progress in Astronautics, Vol. 81, 1982.

[2] Mc Croskey W. Unsteady airfoils. *Annual Review of Fluid Mech.*, Vol. 14, 1982.

[3] Le Balleur J C, Peyret T and Viviand H. Numerical studies in high Reynolds number aerodynamics. *Computers and Fluids*, Vol. 8, No. 1, 1980.

[4] Le Balleur J C. Numerical viscous-inviscid interaction in steady and unsteady flows. *Proceedings of the 2nd Symposium on Numerical and Physical Aspects of Aerodynamic Flows*, Long Beach, CA, 1983.

[5] Le Balleur J C. New possibilities of viscous-inviscid numerical techniques for solving viscous flow equations with massive separation. *Proceedings of the 4th Symposium on Numerical and Physical Aspects of Aerodynamic Flows*, Long Beach, CA, 1989.

[6] Brune G W, Rubbert P E and Forester C K. The analysis of flow fields with separation by numerical matching. *AGARD-CP-168*, 1975.

[7] Cambier L, Ghazzi W, Veuillot J P and Viviand H. A multi-domain approach for the computation of viscous transonic flows by unsteady type methods. *Computational Methods in Viscous Flows*, ed. Habashi W G, Recent Advances in Numerical Methods in Fluids, Vol. 3, 1984.

[8] Le Balleur J C and Girodroux-Lavigne P. Calculation of fully three-dimensional separated flows with an unsteady viscous-inviscid interaction method. *Proceedings of the 5th Symposium on Numerical and Physical Aspects of Aerodynamic Flows*, Long Beach, CA, 1992.

[9] Tabarrok B and Su J. Semi-implicit Taylor-Galerkin finite element methods for incompressible viscous flows. *Computer Methods in Applied Mechanics and Engineering*, Vol. 117, 1994.

[10] Su J, Tabarrok B and Dost S. A time marching boundary element method for two-dimensional incompressible thermally coupled flows. *Computer Methods in Applied Mechanics and Engineering*, Vol. 128, 1995.

[11] Abbott I H and von Doenhoff A E. *Theory of Wing Sections*. Dover Publications, Inc., New York, 1959.

[12] Elkadri N E, Soulaimani A and Deschenes C. A finite element formulation of compressible flows using various sets of independent variables. *Computer Methods in Applied Mechanics and Engineering*, Vol. 181, pp 161-189, 2000.

[13] Dutto L C, Habashi W G and Fortin M. Parallelizable block diagonal preconditioners for the compressible Navier-Stokes equations. *Computer Methods in Applied Mechanics and Engineering*. Vol. 117, pp 15-47, 1994.

[14] Baruzzi G S, Habashi W G and Guevremont J G. A second order finite element method for the solution of the transonic Euler and Navier-Stokes equations. *International Journal for Numerical Methods in Fluids*, Vol. 20, pp 671-693, 1995.

[15] Brooks A N and Hughes T J R. Streamline upwind/Petrov-Galerkin formulations for convection dominated flows with particular emphasis on the incompressible Navier-Stokes equations. *Computer Methods in Applied Mechanics and Engineering*, Vol. 32, pp 199-259, 1982.

[16] Spalart P R and Allmaras S R. A one-equation turbulence model for aerodynamics flows. *AIAA-92-0439*, 1992

[17] Hafez M, South J and Murman E. Artificial compressibility methods for numerical solutions of transonic full potential equation. *AIAA Journal*, Vol. 17, pp 838-844, 1979.


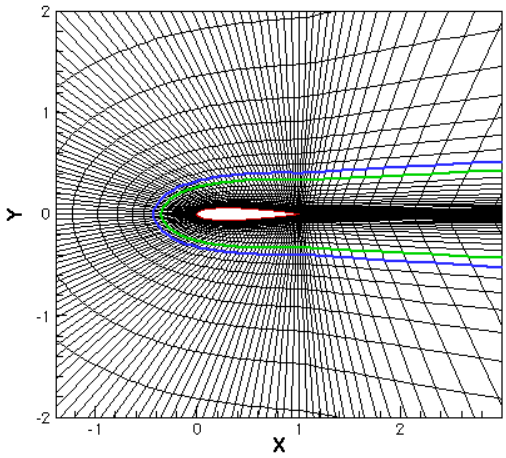


Figure 1. A 151X31 C-grid around an NACA0012 airfoil. The 151X19 grid near the airfoil and its wake is chosen as the viscous zone and the 151X12 grid outside the viscous zone as the inviscid zone.

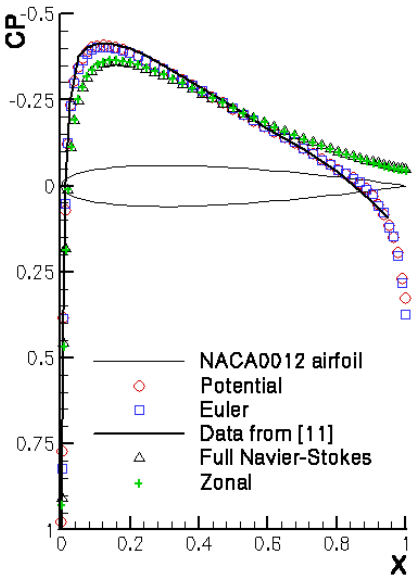


Figure 2. Pressure coefficient over the NACA0012 airfoil at zero angle of attack, Re=6000.

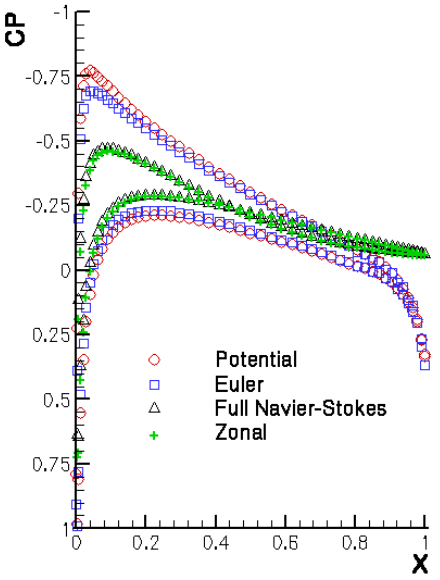


Figure 3. Pressure coefficient over the NACA0012 airfoil at $2^0$ of angle of attack, Re=6000.

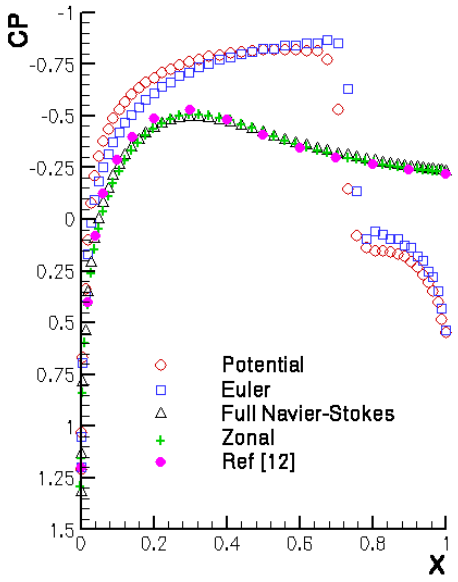


Figure 4. Pressure coefficient over the NACA0012 airfoil at zero angle of attack, $M_\infty$=0.85, Re=2000.

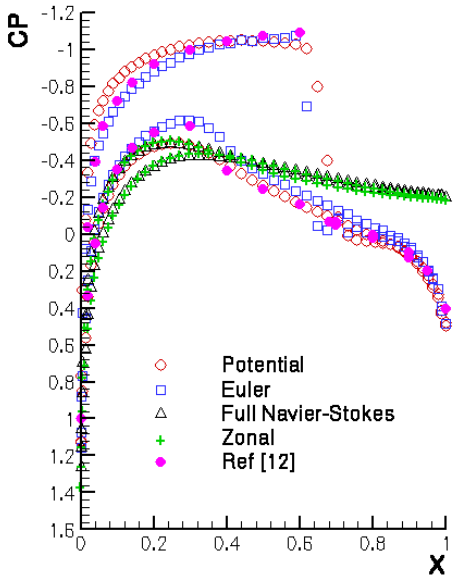


Figure 5. Pressure coefficient over the NACA0012 airfoil at $1.25^0$ of angle of attack, $M_\infty$=0.80, Re=2000.

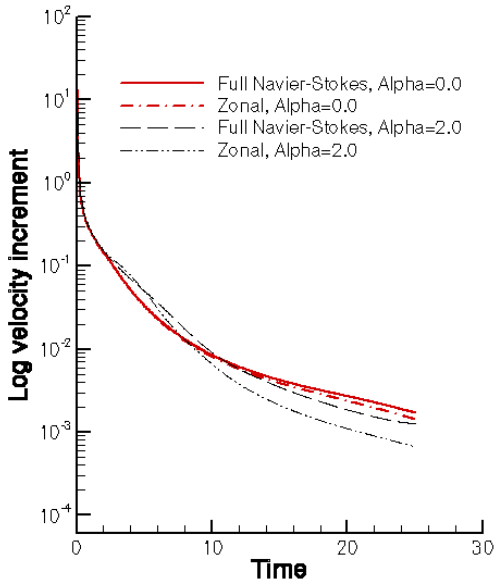


Figure 6. Time history of the velocity increment for incompressible viscous flows

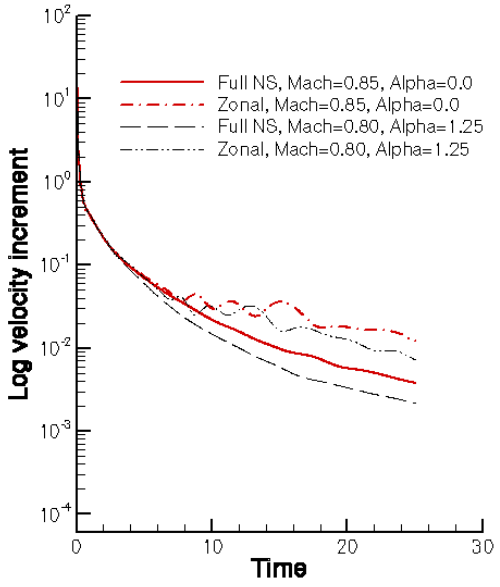


Figure 7. Time history of the velocity increment for compressible viscous flows.